

Universality of Plasmon Excitations in Dirac Semimetals

Dmitri E. Kharzeev,^{1,2} Robert D. Pisarski,^{2,3} and Ho-Ung Yee^{4,3}

¹*Department of Physics and Astronomy, Stony Brook University, Stony Brook, New York 11794-3800, USA*

²*Department of Physics, Brookhaven National Laboratory, Upton, New York 11973, USA*

³*RIKEN-BNL Research Center, Brookhaven National Laboratory, Upton, New York 11973-5000, USA*

⁴*Physics Department, University of Illinois at Chicago, Chicago, Illinois 60607, USA*

(Received 2 February 2015; published 2 December 2015)

We investigate the properties of the collective plasmon excitations in Dirac semimetals by using the methods of relativistic field theory. We find a strong and narrow plasmon excitation whose frequency is in the terahertz (THz) range which may be important for practical applications. The properties of the plasmon appear universal for all Dirac semimetals, due to the large degeneracy of the quasiparticles and the small Fermi velocity, $v_F \ll c$. This universality is closely analogous to the phenomenon of “dimensional transmutation” that is responsible for the emergence of dimensionful scales in relativistic field theories such as quantum chromodynamics.

DOI: 10.1103/PhysRevLett.115.236402

PACS numbers: 71.45.-d

The recent experimental discovery of Cd_3As_2 [1,2] and Na_3Bi [3] Dirac semimetals enables the study of the properties of chiral quasiparticles in three spatial dimensions. As demonstrated by photoemission [1–3], Dirac semimetals are characterized by a linear dispersion relation for fermion quasiparticles, and thus represent three dimensional analogs of graphene. While the distinctive behavior of chiral fermions (*e.g.*, Klein tunneling) is already evident in two dimensional graphene, the physics of chirality in three dimensions opens a number of new possibilities. In particular, the presence of the chiral anomaly in $(3+1)$ dimensional theory should make it possible to observe “chiral magnetic effect (CME)” — a nondissipative current induced by parallel electric and magnetic fields — in such systems; for a review, see [4]. See Refs. [5–7] for other studies of chiral anomaly in Weyl semimetals. The studies of magnetotransport in Cd_3As_2 have already begun [8].

The linear spectrum of quasiparticles also opens new possibilities for photonics or plasmonics. In graphene, which is two dimensional (2D), the plasmon mode does not appear in the random phase approximation (RPA) [9]. A plasmon does arise after doping, or the inclusion of electron-electron interactions, with a plasmon frequency that is in the terahertz (THz) range of frequency [10]. This range is important for diverse practical applications ranging from medical imaging to security.

In this Letter, we investigate the properties of the collective plasmon excitation in three dimensional (3D) Dirac semimetals. Relative to 2D graphene, because of the extra spatial dimension, a strong and narrow plasmon peak already appears in the random phase approximation. At zero chemical potential and for a broad range in temperature, the plasmon frequency is approximately linear in T and is in the THz range at room temperature.

Dirac semimetals are characterized by strong coupling and a large fermion degeneracy, N . We show that this leads to *universal* properties of the plasmon excitation: the plasmon spectrum does not depend on the value of the coupling constant nor upon the degeneracy, N , of the Dirac point. The reason underlying this universality is the quantum scale anomaly of relativistic field theory, where it is known as “dimensional transmutation”. In quantum chromodynamics (QCD), this phenomenon is responsible for the masses of all strongly interacting particles and thus for $\sim 95\%$ of the mass of the visible Universe.

To compute the plasmon spectrum, we need a method valid at strong coupling. This is because for both 3D Dirac semimetals and for 2D graphene, the role of the fine structure constant $\alpha_{em} = e^2/(4\pi\hbar c)$ is played by the effective coupling $\alpha = e^2/(4\pi\hbar v)$, where $v \ll c$ is the Fermi velocity. The Fermi velocity in Cd_3As_2 was experimentally determined [8] to be $v \approx 9.3 \times 10^5$ m/s $\approx 1/300c$, close to the value in graphene. Because of this, the effective coupling constant $\alpha \approx 2.2$ is very large. This is comparable to the value of the strong coupling constant in the quark-gluon plasma, near the deconfining transition in QCD.

Generally, the photon propagator cannot be computed perturbatively in strong coupling. However, there is an alternate expansion possible. The degeneracy factor of fermion quasiparticles is large: due to the degeneracy in the electron spin and double valleys, $N = 4$ for both 3D Dirac semimetals and for graphene. We can then use a large N expansion to compute the photon propagator to leading order in $1/N$. At nonzero temperature and density, the result for the photon propagator is similar to that obtained in the hard thermal loop (HTL) approach to the quark-gluon plasma [11,12]. The HTL approximation is used, *e.g.*, to compute the rate of electromagnetic radiation from the

quark-gluon plasma [13]. In this Letter, we employ similar methods for evaluating the plasmon spectrum and damping rate in Dirac semimetals.

When the number of fermions species N is large, the photon dynamics is dominated by dressing the photon with the one loop fermion diagrams. More precisely, in the effective large N action for the photon, the dominant kinetic term is provided by the large N enhanced self-energy arising from one loop fermion diagram, which gives the leading photon propagator in the large N perturbation scheme. As a result, the photon propagator is suppressed by $1/N$, and photon-mediated interactions are suppressed by $1/N$, so the fermion dynamics are those of a free theory. As long as N is sufficiently large, this remains true even at strong coupling [14]. A similar large N suppression also holds true for higher photon vertices generated by fermion one loop diagrams. Further, we can neglect the scale dependence of the Fermi velocity, as that originates from loop corrections to the fermion propagator. Indeed, for graphene, the suppression of the dependence of the velocity scale with $1/N$ is manifest [15]. One needs to include these $1/N$ corrections to correctly estimate the quality of large N approximation; we leave these studies for future investigations.

In the one loop approximation at large N , the longitudinal Coulomb and the transverse sectors of the plasmon decouple from one another. In the following, we focus on the Coulomb sector. (We note, however, that in the static limit in which we compute, the transverse and Coulomb plasmons are degenerate.) From the above discussion, the effective coupling in the Coulomb sector is

$$\lambda(\Lambda_c) \equiv \frac{Ne^2(\Lambda_c)}{v}. \quad (1)$$

We emphasize here the dependence on the physical UV lattice cutoff Λ_c at which the observed value of the coupling is defined:

$$e^2(\Lambda_c) \simeq \frac{1}{137} \times (4\pi) \approx 0.1. \quad (2)$$

It is well-known that in a gauge theory with massless fermions, there is no intrinsic notion of the coupling constant: the coupling constant changes, or “runs”, as the length scale at which it is probed changes. Hence, one can trade the value of the coupling constant for the dimensionful scale at which it is defined, which is known as “dimensional transmutation”. For our purposes, we can define this scale as that where the coupling blows up, at the Landau pole Λ_L . The physical observables then depend only upon the ratio of an external scale, Q , at which the coupling is measured to Λ_L . At one loop order, the coupling $\lambda(Q)$ at a scale Q is given by

$$\lambda(Q) = \frac{\lambda(\Lambda_c)}{1 - \frac{\lambda(\Lambda_c)}{12\pi^2} \log\left(\frac{Q^2}{\Lambda_c^2}\right)} = \frac{12\pi^2}{\log\left(\frac{\Lambda_L^2}{Q^2}\right)}. \quad (3)$$

The first equality in Eq. (3) contains a Landau pole at $\Lambda_L \equiv \Lambda_c \exp[6\pi^2/\lambda(\Lambda_c)]$, which is where the coupling constant diverges. We can then rewrite this as the second equality in Eq. (3), which shows that the coupling is a function solely of the ratio Q/Λ_L . That is, Λ_c and $\lambda(\Lambda_c)$ are transmuted to a single scale Λ_L , which is the only dimensionful parameter of the theory. This means that at nonzero temperature T and chemical potential μ , any observable in the photon sector is of the form

$$T^\Delta f\left(\frac{T}{\Lambda_L}, \frac{\mu}{T}\right). \quad (4)$$

Here, Δ is the mass dimension of the observable; in this Letter, it is the plasmon frequency, with $\Delta = 1$. The function $f(x, y)$ depends upon the observable in question, but is otherwise universal: all of the dependence on Λ_c and $\lambda(\Lambda_c)$ is included in the single parameter, Λ_L . It is worth emphasizing that neither N or v appears in the function $f(x, y)$. This is most powerful, as it is then possible to find $f(x, y)$ with ease in the one-loop approximation valid at large N . In this Letter, we compute the universal function $f(x, y)$ for the plasmon frequency at zero spatial momentum. It is worth emphasizing that the “vacuum” contribution to the one loop diagram, from zero temperature and density, plays a crucial role in realizing this universality. (This is not captured by the hard thermal loop limit, which neglects the vacuum contribution.)

The limit of strong coupling is defined as follows. Given the physical lattice cutoff, Λ_c , with a fixed $e^2(\Lambda_c) \approx 0.1$, a large value of N/v can give a large value of $\lambda(\Lambda_c)$. Thus, in the strong coupling limit, $\Lambda_L = e^{6\pi^2/\lambda(\Lambda_c)}\Lambda_c \approx \Lambda_c$, any observable in the photon sector at nonzero T and μ becomes

$$T^\Delta f\left(\frac{T}{\Lambda_c}, \frac{\mu}{T}\right), \quad (5)$$

with the *same* function $f(x, y)$. That is, the result is independent of the values of N , v , or $e^2(\Lambda_c) \approx 0.1$. We call this a universality of strong coupling.

For $N = 4$ and $1/v = 300$, we have

$$\lambda(\Lambda_c)/6\pi^2 \approx 2, \quad (6)$$

so that

$$\Lambda_L \approx 1.65\Lambda_c. \quad (7)$$

In spite of the uncertainty in the value of Λ_c , it is thus reasonable to assume that the strong coupling limit, and so Eq. (5), are justified.

Our main novel result is a complete determination of the function $f(x, y)$ for the plasmon frequency ($\Delta = 1$) at zero spatial momentum in one-loop large N approximation. The resulting plasmon exhibits the scaling behavior expected from the quantum dimensional transmutation phenomenon. Our result gives a concrete prediction for the plasmon frequency in Dirac semimetals which has a universal form.

We now turn to a summary of the details of the computation of the plasmon frequency. The plasmon arises from the singularity in the longitudinal component of the retarded photon propagator. In Coulomb gauge, $\vec{\nabla} \cdot \vec{A} = 0$, this propagator is

$$\begin{aligned} \Pi_R^{00}(p) &\equiv \langle A^0(p)A^0(-p) \rangle = \frac{i}{|\mathbf{p}|^2 - \Pi_R^L(p)}, \\ \Pi_R^L(p) &\equiv \langle J^0(p)J^0(-p) \rangle_R. \end{aligned} \quad (8)$$

The one-loop expression for the longitudinal retarded self-energy $\Pi_R^L(p)$ consists of two parts: the first in vacuum, at $T = \mu = 0$, and the second from $T, \mu \neq 0$. The contribution in vacuum is

$$\Pi_R^{\text{vac}}(p) = \frac{Ne^2(\Lambda_c)|\mathbf{p}|^2}{12\pi^2 v} \log\left(\frac{-p^2}{\Lambda_c^2}\right) \Big|_{p^0 \rightarrow p^0 + i\epsilon}, \quad (9)$$

where the square of the four momentum is $p^2 = (p^0)^2 - v^2|\mathbf{p}|^2$ and $\Lambda_c \approx 5 \text{ eV} \approx 10^5 \text{ K}$ for Cd_3As_2 is the ultraviolet cutoff in the energy spectrum of chiral quasiparticles, which is the maximum energy at the boundary of Brillouin zone measured in angle-resolved photoemission spectroscopy (ARPES) experiments. The second part from $T, \mu \neq 0$, after rescaling the spatial momentum integration variable from \mathbf{k} to \mathbf{k}/v , is given by

$$\Pi_R^{\text{th}}(p) = \frac{Ne^2(\Lambda_c)}{2\pi^2 v^3} \int_0^\infty dk k^2 \mathcal{N}(k) I(p, k), \quad (10)$$

where

$$\begin{aligned} I(p, k) &= \int_{-1}^1 dx \left[\frac{2k + p^0 + v|\mathbf{p}|x}{(p^0)^2 - v^2|\mathbf{p}|^2 + 2p^0k - 2v|\mathbf{p}|kx + i\epsilon(k + p^0)} \right. \\ &\quad \left. - \frac{2k - p^0 - v|\mathbf{p}|x}{-(p^0)^2 + v^2|\mathbf{p}|^2 + 2p^0k - 2v|\mathbf{p}|kx + i\epsilon(k - p^0)} \right], \end{aligned} \quad (11)$$

and $\mathcal{N}(k) = [e^{(k-\mu)/T} + 1]^{-1} + [e^{(k+\mu)/T} + 1]^{-1}$ is the sum of the Fermi-Dirac statistical distribution functions for particles and antiparticles (holes). In the limit of small spatial momenta, $\mathbf{p} \rightarrow 0$, that we focus on, $I(p, k)$ becomes

$$I(p, k) \rightarrow \frac{4}{3} \frac{kv^2 p^2}{(p^0)^2 (k + \frac{p^0}{2} + i\epsilon)(k - \frac{p^0}{2} - i\epsilon)} + \mathcal{O}((p^2)^2) \quad (12)$$

The equation for the plasmon frequency, $p^0 = \omega_{pl}$, after changing the integration variable $k \rightarrow \bar{k} = k/T$ and introducing $\bar{\mu} = \mu/T$, is

$$\begin{aligned} (\bar{p}^0)^2 \log \left[-(\bar{p}^0 + i\epsilon)^2 \cdot \frac{T^2}{\Lambda_L^2} \right] \\ + 8 \int_0^\infty d\bar{k} \bar{k}^3 \left(\frac{1}{e^{\bar{k}-\bar{\mu}} + 1} + \frac{1}{e^{\bar{k}+\bar{\mu}} + 1} \right) \\ \times \frac{1}{(\bar{k} + \frac{\bar{p}^0}{2} + i\epsilon)(\bar{k} - \frac{\bar{p}^0}{2} - i\epsilon)} = 0, \end{aligned} \quad (13)$$

where $\bar{p}^0 = p^0/T$. In this expression, all other parameters disappear and are replaced by the single scale $\Lambda_L = e^{6\pi^2/\lambda(\Lambda_c)} \Lambda_c \approx 1.65\Lambda_c$ as discussed before. This shows that the solution for the plasmon frequency takes the form

$$\omega_{pl}(T) = T f(T/\Lambda_L, \mu/T), \quad (14)$$

where the function $f(x, y)$ is universal, independent of the values of the coupling constant $e^2(\Lambda_c)$, degeneracy N , and the Fermi velocity v .

For small $x \equiv T/\Lambda_L$ and $xy \equiv \mu/\Lambda_L$, the function $f(x, y)$ can be found to agree with the HTL method with running coupling constant, depending on the value of $y = \mu/T$. In the case $y \ll 1$, the result is

$$f(x, y) \approx \sqrt{\frac{2(\frac{\pi^2}{3} + y^2)}{\log(1/x)}}, \quad y \ll 1, \quad x \ll 1, \quad (15)$$

and in the case of $y \gg 1$,

$$f(x, y) \approx \sqrt{\frac{2y^2}{\log(1/xy)}}, \quad y \gg 1, \quad xy \ll 1. \quad (16)$$

For a general x and y , $f(x, y)$ is complex valued; we have evaluated it numerically. The imaginary part of $f(x, y)$ is consistently smaller than its real part, which allows us to find the imaginary part in first order perturbation to the real part. Writing

$$f(x, y) = \bar{p}^0 = \frac{\omega_{pl}}{T} - i \frac{\gamma}{T} \equiv \bar{\omega}_{pl} - i\bar{\gamma}, \quad (17)$$

the equation for the real part of $\bar{\omega}_{pl} > 0$ is

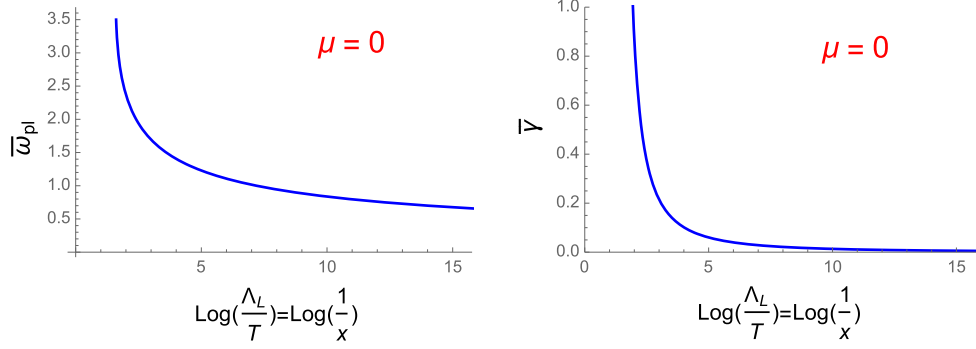


FIG. 1 (color online). The real (left) and imaginary (right) parts of the plasmon energy, divided by the temperature, $f(x) \equiv \omega_{pl}/T - i\gamma/T$, as a function of $\log(\Lambda_L/T) = \log(1/x)$.

$$\bar{\omega}_{pl}^2(\log x + \log \bar{\omega}_{pl}) + 4\mathcal{P} \int_0^\infty d\bar{k} \left(\frac{1}{e^{\bar{k}-y} + 1} + \frac{1}{e^{\bar{k}+y} + 1} \right) \times \frac{\bar{k}^3}{(\bar{k} + \bar{\omega}_{pl}/2)(\bar{k} - \bar{\omega}_{pl}/2)} = 0, \quad (18)$$

where \mathcal{P} denotes a principal value integration. With $\bar{\omega}_{pl}$ found, in linear approximation, the damping rate γ is

$$\bar{\gamma} = -\frac{\pi}{4} \frac{\bar{\omega}_{pl}}{(\log x + \log \bar{\omega}_{pl})} \times \left[1 - \frac{1}{e^{(\bar{\omega}_{pl}/2-y)} + 1} - \frac{1}{e^{(\bar{\omega}_{pl}/2+y)} + 1} \right]. \quad (19)$$

The resulting real and imaginary parts of the plasmon energy, normalized to the temperature T , are presented in Fig. 1 as a function of $\log(\Lambda_L/T) = \log(1/x)$ when $y = \bar{\mu} = 0$.

In Fig. 2, we present the plasmon frequency in physical units of terahertz (THz) as a function of temperature at zero chemical potential and at a chemical potential of $\mu = 200$ meV with $\Lambda_c \approx 5$ eV $\approx 5.8 \times 10^4$ K, which is characteristic for Cd_3As_2 [1,2]. For the case of zero chemical

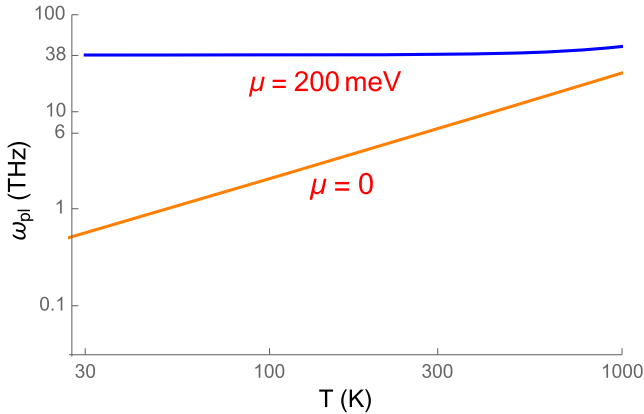


FIG. 2 (color online). The plasmon frequency ω_{pl} as a function of temperature T .

potential, we see that by changing the temperature, the plasmon frequency can be tuned from the radio wave to the near infrared range of the spectrum. In this entire frequency range, the damping of the plasmon is weak, with $\gamma/\omega_{pl} < 0.05$, so the plasmon peak is very narrow.

Let us first estimate numerically the magnitude of the plasmon frequency that we have derived. The UV cutoff in the energy spectrum of quasiparticles indicated by the ARPES measurements in Cd_3As_2 is $\Lambda_c \approx 5$ eV $\approx 5.8 \times 10^4$ K. For the dimensionful scale Λ_L , we thus get $\Lambda_L \approx 1.65\Lambda_c \approx 10^5$ K, see Eq. (7). For the room temperature of $T \approx 300$ K, we get $\log(\Lambda_L/T) \approx 5.7$. Figure 1 then yields the plasmon frequency of $\omega_{pl} \approx T \approx 6$ THz ≈ 0.5 mm $^{-1}$. We have thus found that for room temperature Cd_3As_2 possesses the plasmon in the terahertz frequency range, which may have important applications for THz imaging. It is known that Cd_3As_2 undergoes a phase change at the temperature of $T \approx 888$ K [16]. For this temperature, we get $\log(\Lambda_L/T) \approx 4.7$, and from Fig. 1, the plasmon frequency is still $\omega_{pl} \approx T$, which at this higher temperature yields a higher frequency $\omega_{pl} \approx 18$ THz. At a low temperature of $T = 3$ K, we get $\log(\Lambda_L/T) \approx 10.4$, and from Fig. 1, the plasmon frequency is $\omega_{pl} \approx T$ which yields a low frequency of $\omega_{pl} \approx 60$ GHz ≈ 1 cm $^{-1}$ which is in the radio frequency range.

We should point out that our analysis neglects possible additional contributions to screening, or equivalently, the value of the effective coupling constant at the infrared scale, that are not captured by the quasiparticles with linear dispersion relations. With a typical infrared cutoff $\Lambda_{\text{IR}} = 10$ meV provided either by chemical potential or by the (small) gap in the dispersion relation, our prediction for the dielectric constant from Eq. (3) is

$$\epsilon \equiv \frac{e^2(\Lambda_c)}{e^2(\Lambda_{\text{IR}})} = \frac{Ne^2(\Lambda_c)}{12\pi^2 v} \log\left(\frac{\Lambda_L^2}{\Lambda_{\text{IR}}^2}\right) \approx 11.6, \quad (20)$$

which is about a factor of 3 smaller than the experimental measurement of dielectric constant in Ref. [17]. Since the plasmon frequency depends on these additional screening

effects, only through the value of the coupling constant at the infrared scale, we can accommodate them by effectively rescaling our predictions by $1/\sqrt{3} \approx 0.6$.

Our predictions can be tested experimentally by measuring the plasmon frequency at different temperatures. In realistic systems, there can be several effects that may invalidate our treatment that assumes the absence of mass scales other than dimensional transmutation: for example, a small correction to the linear dispersion relation $p^0 = \sqrt{v^2|\mathbf{p}|^2 + (m + B|\mathbf{p}|^2)^2}$. The presence of such terms involving m and B will affect the result when $T \leq m$ or $T \geq v^2/B$, but should be irrelevant for $v^2/B \gg T \gg m$. We expect that the temperature range that we discuss lies in this validity regime, since the dispersion relation from ARPES measurements looks quite linear in the corresponding energy range. The dominant electron excitations for the plasmon oscillation have the momentum $\mathbf{p} \sim T/v$ with Compton wavelength $\Delta x \sim v/T \sim 270 \text{ \AA}$, and the system size should be larger than this to neglect possible finite size effects. We also point out that our scaling relation Eq. (4) is expected to be violated in the case of Weyl semimetals where the separation of Weyl points in momentum space in general introduces an additional scale in the problem. The plasmon spectrum in Weyl semimetals presents an interesting open problem.

In summary, plasmons in Dirac semimetals provide a link between the quantum dynamics of relativistic field theories and photonics. Depending on the chemical potential, which can be controlled by doping, Dirac semimetals can be used as sensors or emitters of electromagnetic radiation in a broad frequency range, between radio waves, $\sim 100 \text{ GHz}$, and near infrared, 50 THz .

We thank D. Son and M. Stephanov for discussions. This work was supported in part by the U.S. Department of Energy under Contracts No. DE-FG- 88ER40388 and No. DE-AC02-98CH10886.

Note added.—Recently, Ref. [18] appeared which also observed several key features presented in our work. They also considered finite momentum dispersion of plasmons. There also appeared after our preprint an experimental determination of the plasmon frequency in

ZrTe₅ [19] (a known Dirac semimetal [20]), which shows approximately linear dependence of the plasmon frequency in the temperature range between 100 K and 300 K [see Fig. 3(a) of that paper] in agreement with our prediction.

-
- [1] S. Borisenko, Q. Gibson, D. Evtushinsky, V. Zabolotnyy, B. Büchner, and R.J. Cava, *Phys. Rev. Lett.* **113**, 027603 (2014).
 - [2] M. Neupane, S.-Y. Xu, R. Sankar, N. Alidoust, G. Bian, C. Liu, I. Belopolski, T.-R. Chang, H.-T. Jeng, H. Lin *et al.*, *Nat. Commun.* **5**, 3786 (2014).
 - [3] Z. Liu, B. Zhou, Y. Zhang, Z. Wang, H. Weng, D. Prabhakaran, S.-K. Mo, Z. Shen, Z. Fang, X. Dai *et al.*, *Science* **343**, 864 (2014).
 - [4] D. E. Kharzeev, *Prog. Part. Nucl. Phys.* **75**, 133 (2014).
 - [5] G. Basar, D. E. Kharzeev, and H. U. Yee, *Phys. Rev. B* **89**, 035142 (2014).
 - [6] Phillip E. C. Ashby and J. P. Carbotte, *Phys. Rev. B* **89**, 245121 (2014).
 - [7] J. Zhou, H.-R. Chang, and D. Xiao, *Phys. Rev. B* **91**, 035114 (2015).
 - [8] T. Liang, Q. Gibson, M. N. Ali, M. Liu, R. Cava, and N. Ong, *Nat. Mater.* **14**, 280284 (2015).
 - [9] S. Gangadharaiyah, A. Farid, and E. Mishchenko, *Phys. Rev. Lett.* **100**, 166802 (2008).
 - [10] A. Grigorenko, M. Polini, and K. Novoselov, *Nat. Photonics* **6**, 749 (2012).
 - [11] R. Piasarski, *Phys. Rev. Lett.* **63**, 1129 (1989).
 - [12] E. Braaten and R. D. Pisarski, *Nucl. Phys.* **B337**, 569 (1990).
 - [13] E. Braaten, R. D. Pisarski, and T. C. Yuan, *Phys. Rev. Lett.* **64**, 2242 (1990).
 - [14] D. Son, *Phys. Rev. B* **75**, 235423 (2007).
 - [15] I. Aleiner, D. Kharzeev, and A. Tsvelik, *Phys. Rev. B* **76**, 195415 (2007).
 - [16] S. E. R. Hiscocks and C. T. Elliott, *J. Mater. Sci.* **4**, 784 (1969).
 - [17] J.-P. Jay-Gerin, *Solid State Commun.* **21**, 771 (1977).
 - [18] J. Hofmann and S. Das Sarma, *Phys. Rev. B* **91**, 241108 (2015).
 - [19] R. Y. Chen, S. J. Zhang, J. A. Schneeloch, C. Zhang, Q. Li, G. D. Gu, and N. L. Wang, *Phys. Rev. B* **92**, 075107 (2015).
 - [20] Q. Li, D. E. Kharzeev, C. Zhang, Y. Huang, I. Pletikosic, A. V. Fedorov, R. D. Zhong, J. A. Schneeloch *et al.*, arXiv: 1412.6543.